



Diagnostic signature of the compressibility of the inertial-confinement-fusion pusherK. D. Meaney ^{1,*}, Y. H. Kim,¹ H. Geppert-Kleinrath,¹ H. W. Herrmann,¹ L. Berzak Hopkins,² and N. M. Hoffman ¹¹*Los Alamos National Laboratory, Los Alamos, New Mexico, 87545, USA*²*Lawrence Livermore National Laboratory, Livermore, California, 94550, USA*

(Received 12 September 2019; accepted 6 February 2020; published 19 February 2020)

Carbon shell areal density measurements from many types of inertial confinement fusion implosions at the National Ignition Facility (NIF) demonstrate that the final state of the outside portion of the shell is set primarily by capsule coast time, the coasting period between main laser shut off and peak fusion output. However, the fuel areal density does not correlate with the increasing carbon compression. While two-dimensional (2D) radiation-hydrodynamic simulations successfully capture the carbon compression, energy must be added to the simulated fuel-ice layer to reproduce fuel areal density measurements. The data presented demonstrates that the degradation mechanisms that reduce the compressibility of the fuel do not reduce the compressibility of the ablator.

DOI: [10.1103/PhysRevE.101.023208](https://doi.org/10.1103/PhysRevE.101.023208)

The NIF has the goal of achieving ignition: a propagating fusion burn within the context of inertial confinement fusion (ICF) experiments [1]. In ICF implosions, a low- Z (often carbon) shell surrounds a layer of cryogenic deuterium-tritium (DT) ice with DT gas in the center in equilibrium. The spherical capsule is then compressed through ablation of the carbon shell from an x-ray bath driven with an input laser drive. Sustained high ion temperature and DT fuel areal density must be achieved to ignite [2]. The pusher, which compresses the DT fuel and forms the burning hot spot, is a combination of both the DT ice layer and the remaining carbon ablator. Higher pusher areal density drives a higher hot spot pressure [3]. Historically, the pusher compression has been inferred experimentally through the total DT areal density, as measured through the neutron downscatter ratio [4]. The DT areal density is systematically lower than expected by nominal low-mode radiation hydrodynamics simulations [5]. In fact, there is a long-standing discrepancy between 2D HYDRA [6] simulations, which over predict the DT areal density, and the measured values. The *ad hoc* addition of preheat energy to the ice layer decreases compressibility, possibly serving as a surrogate for the effects of hydrodynamic mix [7]. Integrated, high resolution 3D simulations, with ~ 60 J of preheat added to the DT ice layer to approximate ablator-ice mix, do reproduce the experimentally inferred fuel density, with the understanding that the added energy is a placeholder to capture the complex interactions that experimentally degrade the compressibility of the ice layer [8]. The data shown here focuses on NIF shots since 2015 where all implosions are designed with a higher fuel adiabat than those of the lower adiabat, higher gas fill Nation Ignition Campaign implosions. Across these recent implosions since 2015, the DT areal density has remained relatively constant.

The results in this article demonstrate that the carbon ablator areal density, measured with the Gamma Reaction History diagnostic [9], provide new, quantitative information

about the previously unmeasured outer portion of the pusher. The data show that the ablator compression has continued to increase, primarily through a reduction in coast time, defined as the difference between the end of the main laser drive and peak fusion output. This observation gives direct experimental evidence that late time laser energy continues to increase capsule pressure, as seen in the earlier NIC implosions [10], emphasized by Hurricane *et al.* [11] and implemented by Berzak Hopkins *et al.* [12] for the more recent implosions. Implosions with more laser energy driving longer pulses and shorter coast times have higher ablator compression, unlike the unchanging fuel compression. Furthermore, unlike the DT fuel, the compression of the ablator is correctly captured by 2D HYDRA simulations with no added preheat. The measurements demonstrate that the degradation mechanisms that reduce the compressibility of the DT areal density, such as ablator-ice layer mix, do not significantly affect the ablator portion of the pusher.

When 14 MeV DT fusion neutrons are released from the center of the inertial confinement fusion (ICF) capsule, approximately $\sim 0.5\%$ of the neutrons inelastically scatter on carbon atoms in the ablator, elevating the carbon atoms into their first excited nuclear state, which then immediately decay (~ 20 fs) and emit 4.4 MeV γ rays. This carbon γ -ray signal dominates the γ -ray spectrum and is embedded in a continuum background caused by neutrons leaving the ICF capsule and interacting with the surrounding hohlraum and thermal mechanical package structures, which occurs ~ 100 ps later. The Gamma Reaction History (GRH) instrument, located 6 m from the center of the NIF chamber, uses gas as a Cherenkov medium to threshold and measure time-resolved γ signals [13]. Incoming γ rays are converted to relativistic electrons that travel through a gas cell. If the electrons are traveling faster than the speed of light in the medium, then they emit Cherenkov light that is recorded by a fast photomultiplier tube. The speed of light is set by the index of refraction of the gas, which is controlled by a preassigned gas pressure. The GRH has four gas cells. Two use a high-energy threshold to isolate the fusion reaction history using the 16.8 MeV

*meaney@lanl.gov

γ rays from the DT fusion reaction, which has a small branching ratio [14]. The remaining two gas cells are set at 2.9 MeV and 4.5 MeV thresholds to isolate the dominant carbon γ line [15].

Previously, a forward fit [16] was used to evaluate the time history of carbon γ -ray emission by simulating the γ -ray spectrum and has been used to estimate the density profile during fusion burn [17]. In the results presented here, a more straightforward method using direct subtraction [18] has been applied to NIF data since 2015. The amplitude of the carbon signal is calibrated through carbon puck experiments where a known mass and areal density of carbon is placed 6 cm away from an implosion. This calibration (1.2×10^5 carbon γ rays measured on GRH per mg/cm^2 at 1×10^{16} neutrons) is applied to measurements on cryogenic layered DT experiments to deduce the areal density, or carbon ρR , of the ablator at peak fusion output.

The as-configured GRH instrument measured carbon ρR values for 45 DT NIF shots since the start of 2015. These shots span four NIF experimental campaigns that use carbon-based ablators, including the Highfoot [19,20], Bigfoot [21], the high-density carbon (HDC) [12,22,23,24], and the Hybrid B [25] campaigns. This database also represents a wide range of experimental parameters including laser energies, ablator thicknesses, capsule sizes, laser pulse shapes, and different shell dopant percentages. Within this database, the lowest values for the carbon ρR , 200 to $300 \frac{\text{mg}}{\text{cm}^2}$, are measured for smaller capsules with lower laser energy (subscale HDC and Bigfoot shots); values of 300 to $500 \frac{\text{mg}}{\text{cm}^2}$ for full size, higher laser energy shots (Bigfoot, Highfoot, and HDC); and the highest values, 550 to $650 \frac{\text{mg}}{\text{cm}^2}$, for the oversized scale capsules (Hybrid B, large HDC) that are designed to investigate scaling to higher laser energy. Across all these campaigns, there is no observed correlation of the carbon ρR with hot spot and cold fuel radius (as measured by the neutron imaging system [26,27]), shell velocity or laser picket energy, with coefficient of determination (R^2) values of 0.04 and 0.03, 0.17, 0.01, respectively.

The strongest correlation of carbon ρR is with coast time, the time between the end of the laser drive and peak fusion rate. The comparison against coast time across the campaigns, see Fig. 1(a), shows a suggestive downward correlation for each of the campaigns, with an exception for the Highfoot campaign. Our primary interest here, however, is the effect of the coast time on the compression of the carbon portion of the pusher near stagnation time. This late time evolution is convolved with the mass remaining of the carbon ablator, which is set earlier in the capsule evolution. Typically, $>90\%$ of the mass of the carbon shell is ablated off throughout the capsule's evolution. However, most of the ablation occurs before laser drive turn off. The smaller ablator surface area (approximately 0.16 mm^2 imploded compared to the initial $\sim 4 \text{ mm}^2$) and relatively shorter amount of time (0.4 to 1.8 ns of coasting vs the $\sim 7 \text{ ns}$ of laser drive) makes the coast time contribute a negligible amount of ablator mass loss.

Therefore, to better understand the ablator evolution as a function of coast time, we compare the carbon ρR normalized by the mass remaining. The mass remaining is inferred by input energy and velocity scaling of capsules, which is calibrated through surrogate, noncryogenic capsules and then

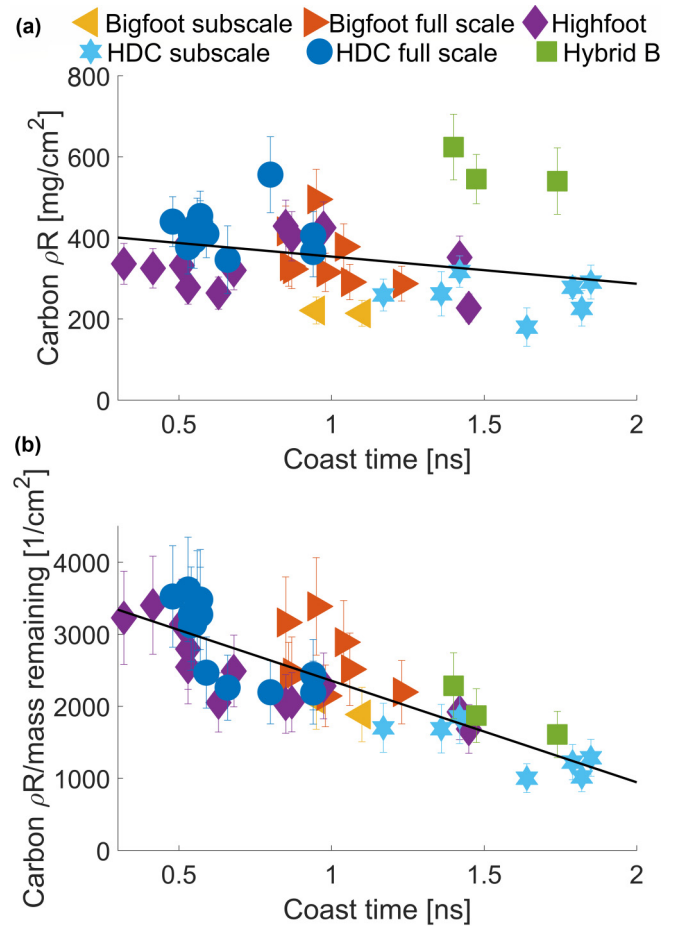


FIG. 1. (a) The measured carbon ρR at peak fusion rate has a suggestive correlation against laser coast time within most campaigns. (b) When corrected by the mass remaining to isolate late time evolution, carbon ρR sees a decreasing correlation with coast time across all campaigns. This effect dominates the carbon ρR value more than any other metric investigated.

applied to the shots that have the DT ice layer [28,29]. Areal density has units of mg/cm^2 and represents the amount of mass integrated radially outward from the center of the capsule. For the normalized, unit mass considered here, the units of $1/\text{cm}^2$ represent an amount of interaction integrated along a path with a set number of carbon atoms. A higher value represents a set number of atoms within a smaller volume and so this value is proportional to the compression of the shell. As an example, the high ρR values in the Hybrid B campaign are due to its higher mass remaining. Correcting by the mass remaining makes it consistent with other campaigns of similar coast time—thus isolating the effect of late-time evolution. Correcting by the mass remaining shows a clear dependence of coast time against carbon ρR across many campaigns [Fig. 1(b)]. The correlation is direct experimental verification that additional late time laser energy continues to maintain a significant pressure on the capsule, in agreement with Hurricane *et al.* [11] and Berzak Hopkins *et al.* [12].

In a series of experiments, laser energy is often increased by extending the laser pulse as opposed to solely increasing peak power. Although coast time is strongly coupled with total laser energy, it is not always a 1-1 relation and the carbon

ρR has a better correlation against coast time than input laser energy (R^2 of 0.7 versus 0.5). This correlation suggests that the laser coast time itself has a direct effect on the ablator compression beyond simply additional laser energy. During the coast time, the hohlraum cools, decreasing the ablation pressure. Decreasing ablation pressure at earlier time, relative to the peak fusion, causes deceleration and in-flight decompression when the shell is at a larger radius. As suggested in stopping power experiments [30], if an early-time decrease of ablation pressure causes the implosion to come in later relative to the coalesced shock, it creates a longer time gap between the shock yield and the compression yield. The rebounding shock then hits the incoming shell at an earlier time (larger radius) and could reduce compression and final areal density. Apart from coast time, increasing dopant percentage is also observed to increase the carbon ρR and overall compression [31]. These effects—increased laser energy, less hohlraum cooling, rarefaction wave, and possibly the rebounding shock hitting the ablator at a larger radius—are all possibilities to contribute to the observed correlation.

The ablator is only part of the total pusher, which is composed of both the remaining ablator and the DT ice layer. The DT ice layer makes up approximately 80% of the total DT ρR . One may naturally hypothesize that the increasing pressure of the ablator, due to shorter coast time and/or more laser energy, should then be communicated to the DT ice layer. The DT ρR is measured by five neutron time of flight instruments [32], which infer the neutron energy spectra. The amount of downscattered neutrons can be related to the total DT ρR through the scattering cross section [4]. However, the DT ρR is uncorrelated with coast time (and laser energy) across all the campaigns (Fig. 2). The Highfoot campaign uses larger capsules that have more initial DT mass, and this is reflected in a higher DT ρR . Once normalized by the DT mass, the Highfoot campaign has an average fuel ρR consistent with other campaigns. The comparison is shown in Fig. 2. The Bigfoot subscale shots have a small amount of DT mass ($90 \mu\text{g}$ compared to $130 \mu\text{g}$) but are observed to have the same fuel ρR as the full scale shots ($\sim 550 \frac{\text{mg}}{\text{cm}^2}$) and consequently indicate an increased efficiency for compressing fuel compared to the other groups. The detailed reason why these subscale shots show increased efficiency is unclear, but the subscale shots also have some of the smallest observed downscattered neutron radii ($\sim 35 \mu\text{m}$ compared to $\sim 45 \mu\text{m}$ for other campaigns) suggesting that these have some of the highest fuel convergence. The overall trend implies that the effects that compress the ablator do not translate directly to the fuel.

Focusing on the HDC campaign, 2D, integrated, HYDRA post-shot simulations that include delivered laser power, as-built hohlraum, capsule and fuel resolved to mode eight with no added preheat successfully capture the carbon ρR variation within the 15% carbon ρR diagnostic measurement uncertainty. Eight HDC post-shot simulations were selected to compare carbon ρR values spanning the coast times and, for these shots, laser energy [33]. Both the absolute values and the observed trend of the carbon ρR and mass corrected carbon ρR are matched by the simulations. However, these 2D HYDRA simulations over-predict the fuel ρR compared to the experimentally inferred values, being on average 30% system-

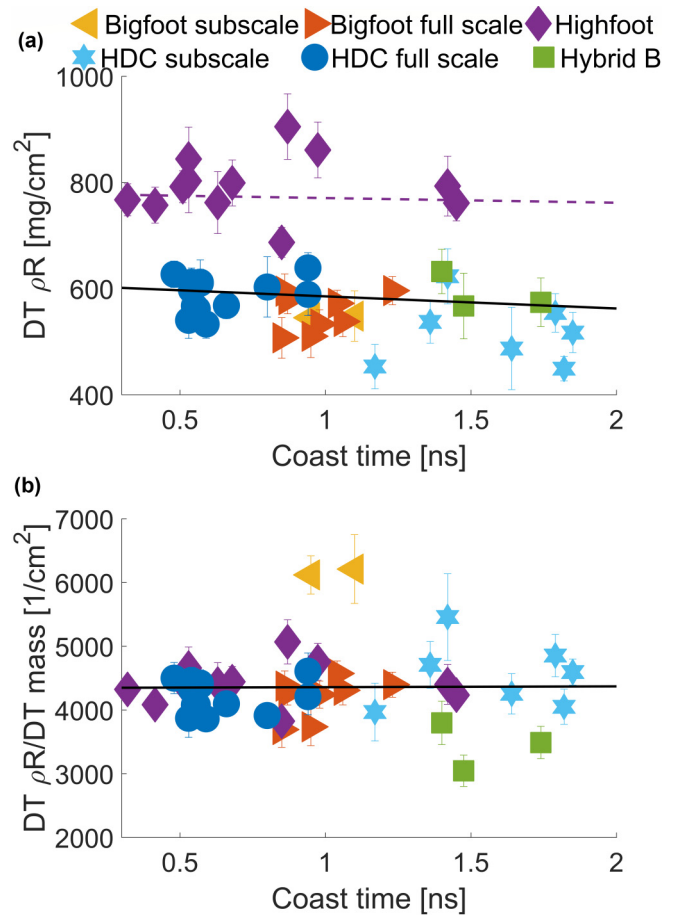


FIG. 2. (a) Unlike the carbon ρR , the fuel ρR has no correlation across coast time. (b) Comparing compression by correcting the fuel ρR with DT mass still shows no correlation with coast time. This implies that the increased compression of the ablator is not being transferred to the rest of the pusher.

atically larger. The fuel ρR has an approximate $\sim 7.5\%$ uncertainty as estimated by the chi squared weighted average from five lines of sight. This overestimation has historically been noted in other ensembles of 2D simulations with the addition of preheat to the simulated ice layer needed to bring the fuel ρR into agreement with measurements [5]. The term “preheat” is used a simulation concept, where joules of energy are added to the DT ice layer to make it less compressible. This knob is a representation of complex degradation mechanisms and is not a specific physics effect. Adding preheat to the DT ice layer in the HYDRA simulations accurately brings the simulated value in line with the experimental value. Shown in a large ensemble of 2D HYDRA simulations, preheat must be added to match observables, including the fuel ρR . Likewise, Clark *et al.*'s [8] high-resolution, 3D Hydra simulations with $\sim 60 \text{ J}$ adiabatically added to the ice layer to replace high-resolution hydrodynamic mix match the experimentally measured fuel ρR . The simulated comparison for both the carbon ρR and the DT ρR corrected by mass are shown in Fig. 3.

Two-dimensional HYDRA simulations over-predict the ice layer compression but successfully capture ablator compression. These results imply that the mechanisms that prevent expected compression of the fuel do not degrade the ablator

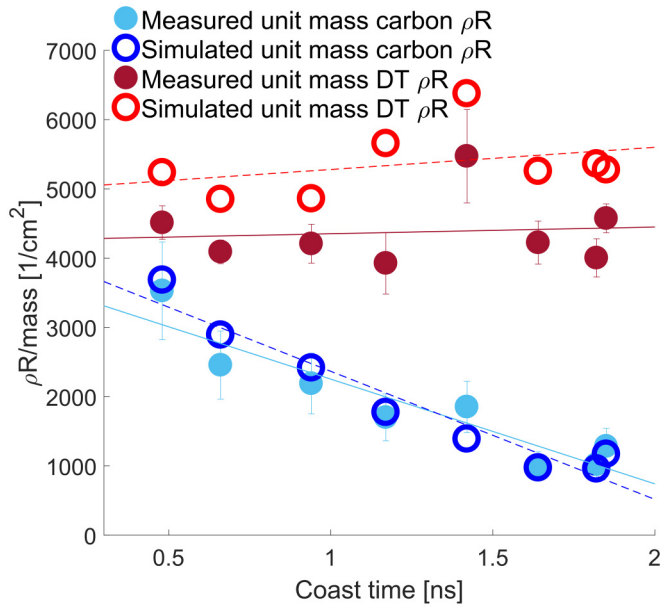


FIG. 3. 2D HYDRA simulations with no preheat capture the ablator compression but overpredict fuel ρR . Adding energy to the ice layer results in the simulation appropriately matching the fuel ρR , suggesting that the ablator profile’s communication to the ice layer is complicated by incompressibility of the DT. The mechanism that makes the DT more incompressible does not significantly affect the compressibility of the ablator portion.

ρR . Cheng *et al.* [34] and Clark *et al.* [8] highlight three potential sources of degradation of fuel compression and yield: mix/preheat in the DT ice layer, perturbations induced by the fuel fill tube, and 3D asymmetries. Experiments have been executed to isolate the effect of different fill tube sizes as well as low mode asymmetries. It is impossible experimentally to isolate the effects between 2D and 3D in the simulations. Therefore, to estimate the effects of 3D asymmetries, large low mode asymmetries, prolate and oblate shapes in both the hot spot and cold fuel, are used as an approximation. These experimental comparisons indicate that neither the fill tube nor asymmetries decrease fuel and carbon ρR . Experiments changing fill tube sizes (2.5 μm , 5 μm , or 10 μm) or having large low mode asymmetries (P2/P0 of +35%, -27%, or -2%) all produce the same carbon ρR and fuel ρR within uncertainty. Because these two effects do not notably decrease pusher compression, it suggests ablator-ice mix to be the main degradation source for the fuel.

Ablator-ice mix has been simulated [35], growth rates of preimposed modulation have been measured [36], and experimental designs seek to minimize its effect [31]. Previous 3D simulations suggested that higher mode resolution ablator-ice mix did not have a significant effect on Highfoot shots [37], but these simulations did not include equation of state variation due to the mix [38]. A DT-carbon mixed material equation of state would be less compressible. In simulations of Highfoot and HDC implosions that match the fuel ρR , ~ 60 J of energy are added to the ice layer adiabatically, with no additional energy added to the ablator portion of the pusher. This evidence supports the practice of adding energy (preheat) to simulate ablator-ice mix solely to the fuel

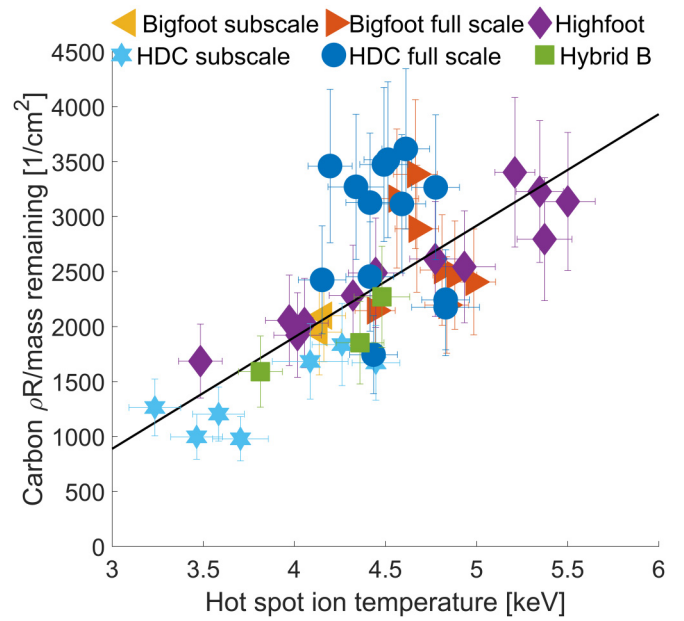


FIG. 4. The compression of the carbon ablator generally correlates with the hot spot ion temperature. Despite the fuel density not having any correlation, increased ablator compression may still improve hot spot confinement, resulting in a higher temperature.

layer and not to include the remaining ablator portion of the pusher. Adding energy to the carbon portion of the shell would decrease the carbon compressibility and give lower carbon ρR than observed. The data suggests that the ablator mix with the DT fuel reduces the compressibility of the fuel but does not significantly affect the remaining ablator compressibility. This observation presents a constraint on the extent and method of ablator-ice mix and models should reflect this observation.

Across these experimental series, the carbon portion of the pusher has continued to increase its compression while the fuel compression remains constant. It is not immediately clear whether increasing pressure from the outer portion of the pusher should then communicate to the hot spot. Theoretical analysis by Hurricane *et al.* [11] suggests that ablation pressure at late time transfers to hot spot, regardless of the density profile or pusher compressibility. We may approximate the hot spot pressure through observables using the Cheng *et al.* [39] hot spot pressure formulation. The derivation gives the form: $P_{\text{HS}} = \frac{4}{5} \frac{(\rho_{\text{HS}})^* R T_{\text{HS}}}{R_{\text{HS}}}$. Aside from the hot spot areal density, these are measured observables. To make an estimate, we make the simplifying assumption that $R_{\text{HS}} \propto \rho R_{\text{fuel}}$, calculate hot spot pressure across these 45 shots and do indeed see a correlation across coast time and inferred hot spot pressure, similar to Ref. [11]. However, both the fuel ρR and the hot spot radius are mostly constant against coast time; it is only the hot spot ion temperature that increases with shorter coast time. Similarly, carbon ρR corrected by mass remaining is correlated with hot spot ion temperature as shown in Fig. 4. Although the hot spot ion temperature can be affected by many factors, this suggests that the increased carbon compression of the pusher may transfer a higher layer temperature to the hot spot despite a less compressible DT layer in the middle. As

Betti *et al.* [3] show, it is the total pusher areal density that increases hot spot pressure, so having a more compressible ice layer by mitigating ablator-ice mix and other degradation mechanisms could be expected to result in further improved performance and fusion output.

In conclusion, measurements of the γ rays scattered from the carbon atoms in the ablator show that the compressibility of the ablator is determined primarily by the laser coast time, a feature captured by 2D HYDRA simulations. This observation verifies that late-time laser energy transfers into an ablation pressure that directly compresses the outer edge of the fuel layer which then communicates with the hot spot pressure. Therefore, the highest performing capsules must be designed with short coast times. The fuel ρR , however, is largely constant and is overestimated by 2D HYDRA simulations, requiring added energy to the simulated ice layer to

reduce its compressibility and match measurements. These data shows that the ablator-ice mix does not significantly affect the ablator areal density, an observation that should help constrain mix models.

We appreciate feedback and foundational work of Charlie Cerjan as well as useful conversations with Art Pak, Omar Hurricane, Nathan Meezan, and Laurent Divol. Thank you to Otto Landen and his NIF data trends tool. We appreciate the hard work of the GRH diagnostic operations team, specifically Jorge Carrera and Eddie Mariscal, as well as the whole NIF operation team. This work was performed under the auspices of the U.S. Department of Energy by LANL under Contract No. DE-AC52-06NA25396. This material was supported by the DOE Office of Science Graduate Student Research (SCGSR) program.

-
- [1] J. D. Lindl, P. Amendt, R. L. Berger, S. Gail Glendinning, S. H. Glenzer, S. W. Haan, R. L. Kauffman, O. L. Landen, and L. J. Suter, *Phys. Plasmas* **11**, 339 (2004).
- [2] C. D. Zhou and R. Betti, *Phys. Plasmas* **15**, 102707 (2008).
- [3] R. Betti, P. Y. Chang, B. K. Spears, K. S. Anderson, J. Edwards, M. Fatenejad, J. D. Lindl, R. L. McCrory, R. Nora, and D. Shvarts, *Phys. Plasmas* **17**, 058102 (2010).
- [4] J. A. Frenje, R. Bionta, E. J. Bond, J. A. Caggiano, D. T. Casey, C. Cerjan, J. Edwards, M. Eckart, D. N. Fittinghoff, and S. Friedrich, *Nucl. Fusion* **53**, 043014 (2013).
- [5] O. A. Hurricane, P. T. Springer, P. K. Patel, D. A. Callahan, K. Baker, D. T. Casey, L. Divol, T. Döppner, D. E. Hinkel, and M. Hohenberger, *Phys. Plasmas* **26**, 052704 (2019).
- [6] S. H. Langer, I. Karlin, and M. M. Marinak, (2015) "Performance Characteristics of HYDRA—A Multi-physics Simulation Code from LLNL," edited by M. Daydé, O. Marques, K. Nakajima In *High Performance Computing for Computational Science—VECPAR 2014*. Lecture Notes in Computer Science, Vol. 8969 (Springer, Cham, 2014).
- [7] J. A. Gaffney, S. T. Brandon, K. D. Humbird, M. K. G. Kruse, R. C. Nora, J. Luc Peterson, and B. K. Spears, *Phys. Plasmas* **26**, 082704 (2019).
- [8] D. S. Clark, C. R. Weber, J. L. Milovich, A. E. Pak, D. T. Casey, B. A. Hammel, D. D. Ho, O. S. Jones, J. M. Koning, A. L. Kritcher *et al.*, *Phys. Plasmas* **26**, 050601 (2019).
- [9] H. W. Herrmann, C. S. Young, J. M. Mack, Y. H. Kim, A. McEvoy, S. Evans, T. Sedillo, S. Batha, M. Schmitt, D. C. Wilson *et al.*, *J. Phys. Conf. Ser.* **244**, 032047 (2010).
- [10] D. G. Hicks, N. B. Meezan, E. L. Dewald, A. J. Mackinnon, R. E. Olson, D. A. Callahan, T. Doppner, L. R. Benedetti, D. K. Bradley, P. M. Celliers *et al.*, *Phys. Plasmas* **19**, 122702 (2012).
- [11] O. A. Hurricane, A. Kritcher, D. A. Callahan, O. Landen, P. K. Patel, P. T. Springer, D. T. Casey, E. L. Dewald, T. R. Dittrich, T. Döppner *et al.*, *Phys. Plasmas* **24**, 092706 (2017).
- [12] L. Berzak Hopkins, S. LePape, L. Divol, A. Pak, E. Dewald, D. D. Ho, N. Meezan, S. Bhandarkar, L. R. Benedetti, T. Bunn *et al.*, *Plasma Phys. Control. Fusion* **61**, 014023 (2019).
- [13] H. W. Herrmann, N. Hoffman, D. C. Wilson, W. Stoeffl, L. Dauffy, Y. H. Kim, A. McEvoy, C. S. Young, J. M. Mack, C. J. Horsfield *et al.*, *Rev. Sci. Instrum.* **81**, 10D333 (2010).
- [14] Y. Kim, J. M. Mack, H. W. Herrmann, C. S. Young, G. M. Hale, S. Caldwell, N. M. Hoffman, S. C. Evans, T. J. Sedillo, A. McEvoy *et al.*, *Phys. Rev. C* **85**, 061601(R) (2012).
- [15] D. B. Sayre, L. A. Bernstein, J. A. Church, H. W. Herrmann, and W. Stoeffl, *Rev. Sci. Instrum.* **83**, 10D905 (2012).
- [16] N. M. Hoffman, H. W. Herrmann, Y. H. Kim, H. H. Hsu, C. J. Horsfield, M. S. Rubery, E. K. Miller, E. Grafil, W. Stoeffl, J. A. Church *et al.*, *Phys. Plasmas* **20**, 042705 (2013).
- [17] C. Cerjan, D. B. Sayre, O. L. Landen, J. A. Church, W. Stoeffl, E. M. Grafil, H. W. Herrmann, N. M. Hoffman, and Y. Kim, *Phys. Plasmas* **22**, 032710 (2015).
- [18] K. D. Meaney, Y. H. Kim, H. W. Herrmann, H. Geppert-Kleinrath, and N. M. Hoffman, *Rev. Sci. Instrum.* **90**, 113503 (2019).
- [19] H.-S. Park, O. A. Hurricane, D. A. Callahan, D. T. Casey, E. L. Dewald, T. R. Dittrich, T. Döppner, D. E. Hinkel, L. F. Berzak Hopkins, S. Le Pape *et al.*, *Phys. Rev. Lett.* **112**, 055001 (2014).
- [20] O. A. Hurricane, D. A. Callahan, D. T. Casey, P. M. Celliers, C. Cerjan, E. L. Dewald, T. R. Dittrich, D. E. H. T. Doppner, L. F. Berzak Hopkins *et al.*, *Nature* **506**, 343 (2014).
- [21] D. T. Casey, C. A. Thomas, K. L. Baker, B. K. Spears, M. Hohenberger, S. F. Khan, R. C. Nora, C. R. Weber, D. T. Woods, O. A. Hurricane *et al.*, *Phys. Plasmas* **25**, 056308 (2018).
- [22] A. J. MacKinnon, N. B. Meezan, J. S. Ross, S. Le Pape, L. Berzak Hopkins, L. Divol, D. Ho, J. Milovich, A. Pak, J. Ralph *et al.*, *Phys. Plasmas* **21**, 056318 (2014).
- [23] S. Le Pape, L. F. Berzak Hopkins, L. Divol, A. Pak, E. L. Dewald, S. Bhandarkar, L. R. Benedetti, T. Bunn, J. Biener, J. Crippen *et al.*, *Phys. Rev. Lett.* **120**, 245003 (2018).
- [24] L. Divol, A. Pak, L. F. Berzak Hopkins, S. Le Pape, N. B. Meezan, E. L. Dewald, D. D.-M. Ho, S. F. Khan, A. J. Mackinnon *et al.*, *Phys. Plasmas* **24**, 056309 (2017).
- [25] A. L. Kritcher, C. Thomas, D. Casey, A. Zylstra, M. Hohenberger, K. Baker, S. Le Pape, D. Clark, C. Weber, M. Stadermann *et al.*, "Hybrid B design and tuning series," 60th

- Meeting of the APS Division of Plasma Physics, Portland, Oregon, Oral Presentation.
- [26] F. E. Merrill, D. Bower, R. Buckles, D. D. Clark, C. R. Danly, O. B. Drury, J. M. Dzenitis, V. E. Fatherley, D. N. Fittinghoff, R. Gallegos *et al.*, *Rev. Sci. Instrum.* **83**, 10D317 (2012).
- [27] P. L. Volegov, C. R. Danly, D. Fittinghoff, V. Geppert-Kleinrath, G. Grim, F. E. Merrill, and C. H. Wilde, *J. Appl. Phys.* **122**, 175901 (2017).
- [28] O. L. Landen, J. Edwards, S. W. Haan, H. F. Robey, J. Milovich, B. K. Spears, S. V. Weber, D. S. Clark, J. D. Lindl, and B. J. MacGowan, *Phys. Plasmas* **18**, 051002 (2011).
- [29] N. B. Meezan, A. J. MacKinnon, D. G. Hicks, E. L. Dewald, R. Tommasini *et al.*, *Phys. Plasmas* **20**, 056311 (2013).
- [30] A. B. Zylstra, J. A. Frenje, F. H. Séguin, D. G. Hicks, E. L. Dewald, H. F. Robey, J. R. Rygg, N. B. Meezan, M. J. Rosenberg, H. G. Rinderknecht *et al.*, *Phys. Plasmas* **21**, 112701 (2014).
- [31] L. Berzak Hopkins, L. Divol, C. Weber, S. Le Pape, N. B. Meezan, J. S. Ross, R. Tommasini, S. Khan, D. D. Ho, J. Biener *et al.*, *Phys. Plasmas* **25**, 080706 (2018).
- [32] V. Yu. Glebov, T. C. Sangster, C. Stoeckl, J. P. Knauer, W. Theobald, K. L. Marshall, M. J. Shoup III, T. Buczek, M. Cruz, T. Duffy *et al.*, *Rev. Sci. Instrum.* **81**, 10D325 (2010).
- [33] The eight shots compared were N160120, N160223, N160418, N161023, N161113, N170601, N180422, and N181014.
- [34] B. Cheng, T. J. T. Kwan, Y. M. Wang, F. E. Merrill, C. J. Cerjan, and S. H. Batha, *Phys. Plasmas* **22**, 082704 (2015).
- [35] D. S. Clark, S. W. Haan, A. W. Cook, M. J. Edwards, B. A. Hammel, J. M. Koning, and M. M. Marinak, *Phys. Plasmas* **18**, 082701 (2011).
- [36] C. R. Weber, T. Döppner, D. T. Casey, T. L. Bunn, L. C. Carlson, R. J. Dylla-Spears, B. J. Kozioziemski, A. G. MacPhee, A. Nikroo, H. F. Robey *et al.*, *Phys. Rev. Lett.* **117**, 075002 (2016).
- [37] D. S. Clark, C. R. Weber, J. L. Milovich, J. D. Salmonson, A. L. Kritcher, S. W. Haan, B. A. Hammel, D. E. Hinkel, O. A. Hurricane, O. S. Jones *et al.*, *Phys. Plasmas* **23**, 056302 (2016).
- [38] D. S. Clark, A. L. Kritcher, J. L. Milovich, J. D. Salmonson, C. R. Weber, S. W. Haan, B. A. Hammel, D. E. Hinkel, M. M. Marinak, M. V. Patel, and S. M. Sepke, *Plasma Phys. Control. Fusion* **59**, 055006 (2017).
- [39] B. Cheng, T. J. T. Kwan, Y.-M. Wang, and S. H. Batha, *Phys. Rev. E* **88**, 041101(R) (2013).